Buckling instability in ordered bacterial colonies

Phys. Biol. **8** (2011) 026008 (7pp) doi:10.1088/1478-3975/8/2/026008

Buckling instability in ordered bacterial colonies

Denis Boyer[1,2,6], **William Mather**[3,6], **Octavio Mondragón-Palomino**[3], **Sirio Orozco-Fuentes**[2], **Tal Danino**[3], **Jeff Hasty**[3,4,5] **and Lev S Tsimring**[5,7]

[1] Laboratoire de Physique Théorique, IRSAMC, CNRS UMR 5152, Université Paul Sabatier, 31062 Toulouse, France
[2] Instituto de Física, Universidad Nacional Autónoma de México, DF 04510, Mexico
[3] Department of Bioengineering, University of California, San Diego, La Jolla, CA 92093-0412, USA
[4] Molecular Biology Section, Division of Biology, UCSD, 9500 Gilman Drive, La Jolla, CA 92093-0368, USA
[5] Biocircuits Institute and San Diego Center for Systems Biology, University of California, San Diego, La Jolla, CA 92093-0328, USA

E-mail: ltsimring@ucsd.edu

Received 1 May 2010
Accepted for publication 26 January 2011
Published 1 March 2011
Online at stacks.iop.org/PhysBio/8/026008

Abstract
Bacterial colonies often exhibit complex spatio-temporal organization. This collective behavior is affected by a multitude of factors ranging from the properties of individual cells (shape, motility, membrane structure) to chemotaxis and other means of cell–cell communication. One of the important but often overlooked mechanisms of spatio-temporal organization is direct mechanical contact among cells in dense colonies such as biofilms. While in natural habitats all these different mechanisms and factors act in concert, one can use laboratory cell cultures to study certain mechanisms in isolation. Recent work demonstrated that growth and ensuing expansion flow of rod-like bacteria *Escherichia coli* in confined environments leads to orientation of cells along the flow direction and thus to ordering of cells. However, the cell orientational ordering remained imperfect. In this paper we study one mechanism responsible for the persistence of disorder in growing cell populations. We demonstrate experimentally that a growing colony of nematically ordered cells is prone to the *buckling instability*. Our theoretical analysis and discrete-element simulations suggest that the nature of this instability is related to the anisotropy of the stress tensor in the ordered cell colony.

S Online supplementary data available from stacks.iop.org/PhysBio/8/026008/mmedia

1. Introduction

Bacteria and other microorganisms often aggregate in dense communities, either on surfaces (biofilms), or in narrow cavities or crevices [1]. In these cases, long-range signaling may play a secondary role in controlling colony organization, whereas direct biomechanical interaction may become the dominant factor [2–4]. Moreover, the lack of free space impedes the flagellae-mediated motility of bacteria in dense colonies such as biofilms, and as a result, the flagellum expression itself is dramatically downregulated [5]. In our recent work [6, 7] we explored the role of biomechanical cell–cell interaction in colony organization using a non-motile strain of bacteria *Escherichia coli* in an open microfluidic chamber (see also [8]). We showed that an expansion flow generated by the cell growth leads to ordering of cells in the direction of the flow. The mechanism of this alignment is different from the alignment of self-propelled particles studied in a number of recent publications (see, for example, [9, 10]) since bacteria were not self-propelled and could only move and change direction under direct mechanical contacts with the

[6] These authors contributed equally to this work.
[7] Author to whom any correspondence should be addressed.

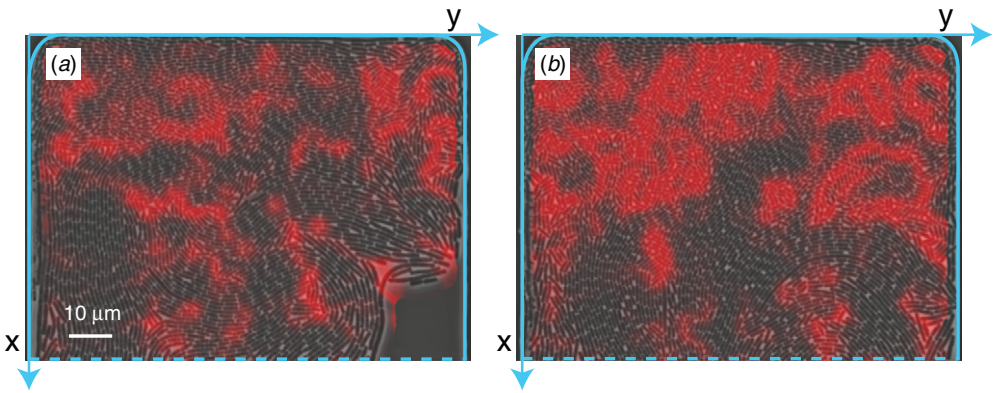

Figure 1. Two snapshots with superimposed local order parameter from the experimental run in a 100×90 μm^2 side trap in which buckling instability was observed: (*a*) $t = 0$ min, (*b*) $t = 25$ min. Solid blue lines show the solid walls of the trap and the dashed blue lines show the open side. Red indicates low values of the local order parameter.

neighboring cells. We found however that in large colonies the perfect nematic order is never reached; multiple domains with different orientations are constantly regenerated in the bulk of the colony. In this paper we focus on the physical mechanism that causes this persistent disorder. We demonstrate that destruction of perfect nematic order occurs due to the *buckling instability* of oriented rod-like cells that is triggered by the expansion flow which creates anisotropic stress tensor in the bulk of the cell colony. We begin with the experimental demonstration of the buckling instability in a quasi-two-dimensional microfluidic trap filled with rod-like *E. coli* cells. We show that the buckling instability occurs in the back of the trap where the density of cells and the pressure are greatest. Then we propose a continuum theoretical description of the buckling instability based on the equations of elasticity theory [11, 12] suitably modified to account for the cell growth. This theory yields buckling instability of a nematically ordered 'cell fluid' at sufficiently high anisotropic pressure compressing the cells along their nematic axis. Because of the expanding flow of cells, the unstable eigenmodes are localized in the interior of the domain where the pressure is sufficiently large. Finally, we present the results of discrete-element simulations (DES) of growing and dividing granular rods which also demonstrate the buckling instability in two-dimensional cell colonies in agreement with the theory and experiments.

2. Experiment

We used a K-12 strain of non-motile bacteria *E. coli* that possess a rod-like structure with a diameter of approximately 1 μm and a length that varies between 2 and 5 μm. The experimental setup used in this work is similar to the one described in [7]. The cells were loaded into custom-designed microfluidic cavities containing shallow (height 1 μm) rectangular 'traps' with (one or more) open sides allowing cells to escape into a deep (height 6 μm) open channel once the trap is densely packed. The latter also served for the delivery of nutrients to cells and for removal of waste. The evolution of the bacterial colony was recorded using optical time-lapse microscopy with 1 min temporal resolution. Several representative movies illustrating colony development are available online (see the supplementary information available at stacks.iop.org/PhysBio/8/026008/mmedia).

We analyzed the bright-field data using the image analysis software ImageJ [13] and code written in MATLAB (MathWorks, Inc.). Cell identification was achieved by background-subtraction and subsequent thresholding of the phase contrast images, with connected regions in the binary mask identified as cell 'particles'. From these regions, we produce a set of centroid positions $\langle\vec{x}\rangle_k$ and angles θ_k for each particle k.

We define the angle θ of a cell particle as the angle of the two-dimensional orthogonal transformation $O_{ij}(\theta)$ that diagonalizes the particle covariance matrix $M_{ij} = \langle x_i x_j\rangle_k - \langle x_i\rangle_k\langle x_j\rangle_k$ (with averages over pixels which belong to the particle with index k) to have the largest eigenvalue in the first component. That is,

$$O_{ij}(\theta) = \cos\left(\theta + (i-j)\,\pi/2\right) \tag{1}$$

such that

$$\sum_{m=1}^{2}\sum_{n=1}^{2} O_{im}^{-1}\, M_{mn}\, O_{nj} = \sigma_i^2\,\delta_{ij} \tag{2}$$

with δ_{ij} the Kronecker delta, and $\sigma_1^2 \geqslant \sigma_2^2$. Thus, $\theta = 0$ for an ellipse with its major axis along the x_1 direction.

The local scalar order parameter η at coordinate $\vec{x}$ and time t was computed in the following manner. Each particle k was assigned an unnormalized Gaussian density

$$\rho_k(\vec{x}) = \exp\left(-\frac{(\vec{x}-\langle\vec{x}\rangle_k)^2}{2\zeta^2}\right) \tag{3}$$

with $\zeta = 1.5$ μm. Using this density, we define the local order parameter

$$\eta(\vec{x}) = \left(\frac{\sum_k \cos(2\theta_k)\,\rho_k(\vec{x})}{\sum_k \rho_k(\vec{x})}\right)^2 + \left(\frac{\sum_k \sin(2\theta_k)\,\rho_k(\vec{x})}{\sum_k \rho_k(\vec{x})}\right)^2. \tag{4}$$

Note that $0 \leqslant \eta \leqslant 1$, where $\eta \approx 0$ in the disordered state (randomly oriented cells) and $\eta \approx 1$ in the ordered state (perfectly aligned cells).

Figure 1 shows a series of snapshots of the cell colony inside a rectangular 100×90 μm^2 trap with one (bottom) side

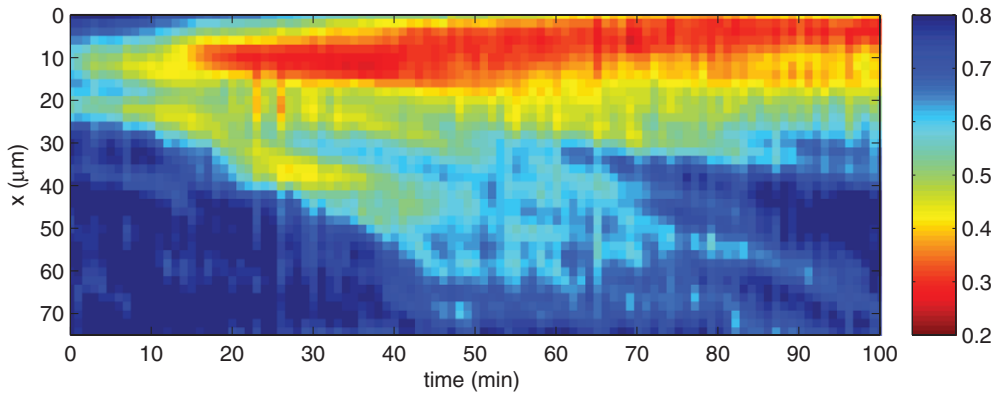

Figure 2. Spacetime diagram of the local order parameter η averaged over the width of the trap for the run illustrated by figure 1.

open. The images are superimposed with the grayscale (color online) distribution of the local orientational order parameter $\eta(\vec{x})$. As seen from this sequence, soon after the colony completely fills the trap, the local order parameter tends to be lower in the back of the trap. This is clearly confirmed by the spacetime plot in figure 2 in which the local order parameter has been averaged over the width of the trap. Interestingly, this plot shows convective propagation of the order parameter with the cell flow from the interior toward the open boundary. We performed a similar analysis for other runs in different trap geometries, and in all of them we observed the reduction of nematic order in the interior of the growing cell colony. Comparison of the bright-field images near the open trap boundary and the interior reveals a strikingly different structure of the colony: while near the open boundary the cells continue to be locally aligned, the nematic order is destroyed in the back of the trap. In the following sections we argue that this phenomenon may be interpreted as a result of the *buckling instability* of nematically ordered population of cells under anisotropic loading which is generated by the cell growth.

3. Continuum modeling

3.1. Preliminaries

In this section we neglect the granularity of the cell population and characterize the cell 'fluid' by the continuum field variables, density $\rho(\mathbf{r}, t)$ and velocity $\mathbf{v}(\mathbf{r}, t)$. Here we consider a rectangular trap of length L_x and width L_y, with two open sides at $x = \pm L_x/2$ and two lateral walls at $y = \pm L_y/2$. The boundary condition $\boldsymbol{\sigma} = 0$ is applied at the open trap sides ($x = \pm L$), where $\boldsymbol{\sigma}$ is the stress tensor [11]. The particles experience a friction force, $-\mu\mathbf{v}$, where μ is the friction coefficient due to bottom and top walls. For simplicity, we neglect friction with the side walls of the trap and intracellular friction.

We also assume that when cells are densely packed, the 'cellular fluid' is incompressible with unit areal density, so the continuity with the volumetric exponential growth at the rate a yields

$$\nabla \cdot \mathbf{v} = a. \tag{5}$$

Since we are interested in the dynamics of initially highly ordered cell population, we regard the system as a packed assembly of elastic columns of rods initially oriented along the x coordinate. Local perturbations can be described by the displacement field $\mathbf{u}$ whose components u_x, u_y are functions of x, y and time t.

3.2. Non-growing compressed rods

Before proceeding to the analysis of the system of growing rods, let us first consider a simpler auxiliary problem of buckling of perfectly ordered *non-growing* rods ($a = 0$) which are compressed along the x coordinate with constant compression p_x. A highly ordered static cell population can be considered a two-dimensional uniaxial solid which can bend in the y direction. The corresponding elastic free energy has the form

$$F_{\mathrm{el}} = \frac{1}{2}\int \mathrm{d}\mathbf{r}\big[\lambda_{xx}u_{xx}^2 + \lambda_{yy}u_{yy}^2 + \lambda_{xy}u_{xy}^2 + \lambda_1 u_{xx}u_{yy} + \xi\left(\partial_x^2 u_y\right)^2\big], \tag{6}$$

where

$$u_{ij} = \tfrac{1}{2}(\partial_j u_i + \partial_i u_j + \partial_i u_k \partial_j u_k) \tag{7}$$

is the Eulerian strain tensor (see [11, 12]) and the last term describes bending elasticity (with the bending constant ξ) of the cell 'columns' (see the supplementary information available at stacks.iop.org/PhysBio/8/026008/mmedia for the calculation of ξ for spherocylindrical 'cells'). The nonlinear term in equation (7) must be retained for large displacements compared to the rod diameter. The components of the stress tensor can be computed by differentiating the elastic free energy with respect to the strain tensor components, $\sigma_{ij} = \delta F/\delta u_{ij}$. In the following we assume that cells have zero Poisson ratio and drop the term proportional to λ_1.

In the unperturbed nematically ordered system there is only one nonzero component of the strain tensor, $u_{xx} = \sigma_{xx}/\lambda_{xx} = -p_x/\lambda_{xx}$ which corresponds to the uniform compression along the x coordinate, respectively. Now we add a small additional non-uniform lateral displacement, $\tilde{u}_y(x)$, assuming that $\partial_x \tilde{u}_y \ll 1$. We first consider the system unbounded in the y direction, and the perturbation $\tilde{u}_y$

independent of y. In this case the free energy can be simplified as

$$F_{el} = \frac{1}{2}\int \mathrm{d}\mathbf{r}\left[\lambda_{xx}u_{xx}^2 + \lambda_{xy}u_{xy}^2 + \xi\left(\partial_x^2\tilde{u}_y\right)^2\right], \tag{8}$$

with the strain tensor

$$u_{xx} = -p_x/\lambda_{xx} + \tfrac{1}{2}(\partial_x\tilde{u}_y)^2, \quad u_{xy} = \tfrac{1}{2}(\partial_x\tilde{u}_y + \partial_y u_x). \tag{9}$$

Substituting (9) into the free energy (8), we obtain

$$F_{el} = \frac{1}{2}\int \mathrm{d}\mathbf{r}\left[p_x^2/\lambda_{xx} - p_x(\partial_x w)^2 + \frac{1}{4}\lambda_{xy}(\partial_x w)^2 + \xi\left(\partial_x^2 w\right)^2\right] \tag{10}$$

(here we introduced the notation $w = \tilde{u}_y$). Thus, while shear and bending elasticity (third and fourth terms in the integrand) increase elastic energy for lateral cell displacements, the second term reduces it due to the release of the longitudinal compression energy. For sufficiently large compression p_x, the reduction is greater than the gain of energy, and buckling instability occurs. This is analogous to the classical Euler buckling instability [11].

In order to describe the dynamics of buckling we form the Lagrangian

$$L = \frac{1}{2}\int \mathrm{d}\mathbf{r}\,\dot{w}^2 - F_{\mathrm{el}} \tag{11}$$

and write down the Euler–Lagrange equation taking into account the dissipation due to the bottom friction

$$\frac{\partial}{\partial t}\left(\frac{\delta L}{\delta \dot{w}}\right) - \frac{\delta L}{\delta w} = -\frac{\delta F_d}{\delta \dot{w}} \tag{12}$$

where $F_d = \mu\int \mathrm{d}\mathbf{r}(\dot{w})^2/2$ is the dissipation function [14]. In the overdamped limit, we can neglect the kinetic energy in the Lagrangian and arrive at the equation for w

$$\mu\partial_t w = (\lambda_{xy}/4 - p_x)\partial_x^2 w - \xi\,\partial_x^4 w. \tag{13}$$

It is easy to see that for sufficiently strong compression ($p > \lambda_{xy}/4$) the system of rods becomes unstable with respect to sufficiently long-wave perturbations. Indeed, substituting $w(x,t) = w_0\exp[st + \mathrm{i}kx]$ in equation (13), we obtain the dispersion relation

$$s = \mu^{-1}[(p_x - \lambda_{xy}/4)k^2 - \xi k^4] \tag{14}$$

which yields the critical wavenumber for the buckling instability $k_c = [(p_x - \lambda_{xy}/4)/\xi]^{1/2}$. Thus, the instability can only occur in sufficiently long traps with length $L_x > 2\pi/k_c$.

For a finite-width trap limited by solid side walls at $y = \pm L_y$ one has to impose the boundary condition $w = 0$ at $y = \pm L_y/2$ and take into account the dependence of w on y. A straightforward generalization of the above derivation leads to the following equation for the local deflection angle:

$$\mu\partial_t w = (\lambda_{xy}/4 - p)\partial_x^2 w - \xi\,\partial_x^4 w + \lambda_{yy}\partial_y^2 w. \tag{15}$$

The growth rate s for the lowest y-mode, $w(x,t) = w_0\exp[st + \mathrm{i}kx]\cos(\pi y/L_y)$ is given by

$$s = \mu^{-1}\left[(p - \lambda_{xy}/4)k^2 - \xi k^4 - \pi^2\lambda_{yy}/L_y^2\right]. \tag{16}$$

The growth rate is lowered by the constant $\pi^2\lambda_{yy}/L_y^2$, and thus the buckling instability is suppressed in narrow traps, as can be expected.

3.3. Growing rods

Here we return to the case where the cells are aligned along the x axis in a rectangular domain $L_x \times L_y$ and they are growing with the rate a and dividing when their size doubles. In the continuum limit, the cell 'medium' is expanding along x with the rate a, which due to mass conservation, equation (5), corresponds to the x-component of velocity $v_x = ax$. In the first approximation the effect of this expansion flow can be captured by adding the convective term $v_x\partial_x w$ to the left-hand side of equation (13). Furthermore, the compression σ_{xx} now is not externally imposed but is internally generated by the cell growth. Since in the overdamped limit $v_x = -\mu^{-1}\partial_x p_x$, one deduces $p_x = \frac{1}{2}\mu a(x^2 - L_x^2/4)$, where the condition $p_x(\pm L_x/2) = 0$ has been used. Substituting this pressure, we obtain

$$\partial_t w + ax\partial_x w = -\left[\frac{a}{2}\left(L_x^2/4 - x^2\right) - \lambda_{xy}/4\mu\right]\partial_x^2 w - \frac{\xi}{\mu}\partial_x^4 w \tag{17}$$

(here we again consider an infinite domain in the y direction, $L_y \to \infty$).

This equation has to be augmented by the boundary conditions at $x = \pm L_x/2$. In analogy to the beam equations, the absence of stress and torque near the free boundaries leads to the boundary conditions $\partial_{xx} w = 0$, $\partial_x^3 w = 0$. Now we can look for exponentially growing solutions in the form $w = \exp(st)f(x)$. Using rescaled variables $16t\xi/\mu L_x^4 \to t$ and $2x/L_x \to x$, we obtain the eigenvalue problem

$$\begin{aligned} sw &= -a_* x w' - \frac{a_*}{2}(1 - x^2)w'' - w'''', \\ w''(\pm 1) &= w'''(\pm 1) = 0 \end{aligned} \tag{18}$$

with one non-dimensional parameter $a_* = a\mu L_x^4/16\xi$. It is easy to show that in the limit $a_* \to 0$, all eigenvalues s_n are negative. However, for a finite a_* eigenvalues can cross zero, which would signify the onset of buckling instability. It is straightforward to compute eigenmodes and eigenvalues numerically by continuation from $a_* = 0$ to finite a^* using Maple continuation routine (Waterloo Maple, Inc.). Figure 3 shows the first five eigenvalues $s_1, \ldots, s_5$ of odd ($w_n^o(x) = -w_n^o(-x)$) and even $\left(w_n^e(x) = w_n^e(-x)\right)$ modes as a function of a^* and an example of lowest unstable eigenmodes $w_1^{e,o}(x)$ for $a_* = 2500$. In the original non-rescaled variables, for odd modes the buckling bifurcation occurs at $a\mu L_x^4/16\xi \approx 63$ and for even modes at $a\mu L_x^4/16\xi \approx 62$, i.e. for sufficiently large growth rate a or system size L, or friction μ. As seen in figure 3(*b*), the eigenmodes are large in the middle of the trap and become very small near the open ends, which indicates that unstable perturbations are mostly confined to the interior of the trap, where growth-generated pressure is sufficiently high. This agrees well with our experimental findings as well as with discrete-element simulation described in the next section.

Similarly to the case of non-growing rods above, the finite transversal width of the trap reduces the eigenvalues by the fixed value $\pi^2\lambda_{yy}/4L_y^2$, see equation (16), whereby increasing the threshold growth rate (or longitudinal system size) necessary for the onset of the buckling instability.

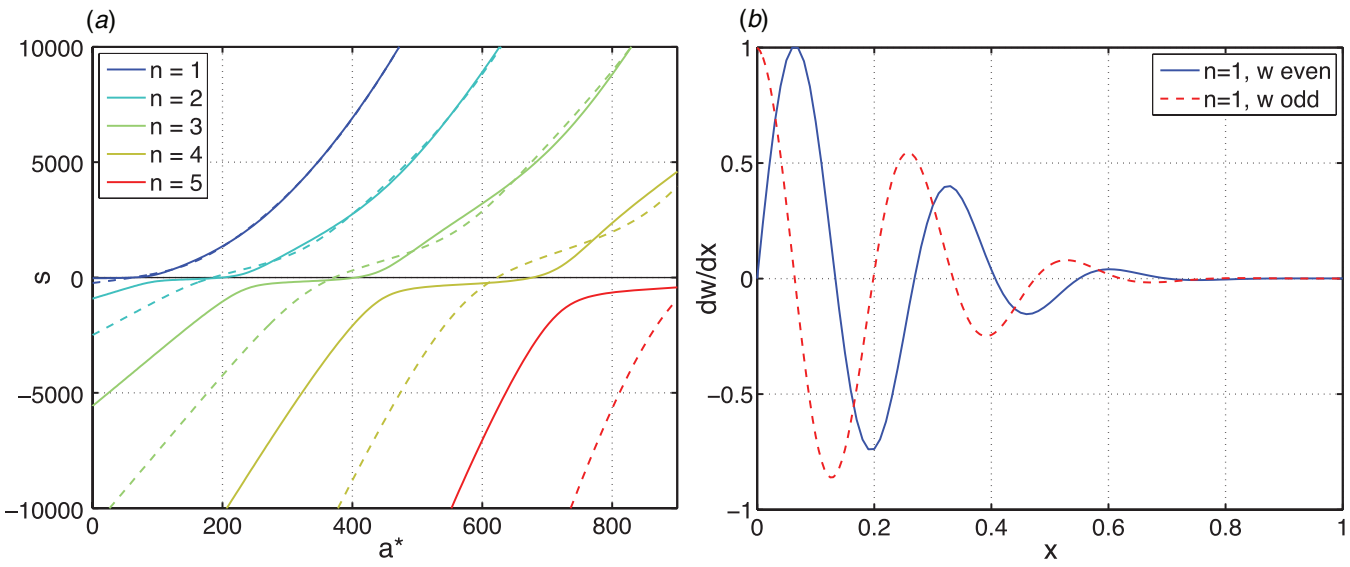

Figure 3. (*a*) First five eigenvalues corresponding to odd (dashed) and even (solid) modes of equation (17) as functions of a_*. (*b*) Two fastest growing eigenmodes (even $w_0^e(x)$ and odd $w_0^o(x)$) for $a_* = 2500$ corresponding to almost identical positive (unstable) eigenvalues $s_0 = 3.4737\ldots \times 10^5$.

4. Discrete-element simulations

To further investigate the nature of the buckling instability and gain insight in the asymptotic regime which emerges after the buckling instability develops, we performed discrete-element soft-particle simulations of a quasi-two-dimensional monolayer of growing and dividing cells. The numerical algorithm for these simulations has been described previously [6, 7]. Each cell is represented by a spherocylinder with fixed diameter d and variable length l that grows exponentially until it reaches a certain critical length $l_{\rm div}$ at which the cell is replaced by two collinear cells of equal length $l_{\rm div}/2$. The critical length $l_{\rm div}$ is chosen randomly at the birth of the cell from a distribution centered at a certain l_0 to avoid spurious synchronization of cell divisions across population. It is possible to establish a connection between microscopic parameters of the spherocylinders and the rheological parameters used in continuum description of the previous section (see the supplementary information available at stacks.iop.org/PhysBio/8/026008/mmedia); however, certain details of the simulations related to the granularity of the medium evidently cannot be adequately captured by the continuum theory. The normal and tangential (frictional) forces moving the cells are computed based on the overlap of virtual soft spheres centered at the nearest points on the axes of interacting spherocylinders. These contact forces and 'bottom friction' force between cells and the substrate are then used to compute the motion of cells by integrating Newton's equations. As soon as the cell center of mass crosses one of the open boundaries, the cell is removed from the pool. The microscopic parameters characterizing the elastic and dissipative properties of the cells coincide (unless indicated) with the ones used in [6, 7].

We performed simulations for two types of geometries: 'open traps' with two solid side walls at $y = 0, L_y$ and two open boundaries at $x = 0, L_x$ and 'side traps' with three solid walls at $y = 0, L_y$ and $x = L_x$ and only one open boundary at $x = L_x$, similar to the experimental realization shown in figure 1. We carried out simulations with different cell aspect ratios $A = l_0/d$ and system sizes L_x, L_y.

A typical 'open trap' simulation for rods with the mean aspect ratio at division $A = 6$ is illustrated by figure 4 (see also movie 3 in the supplementary information available at stacks.iop.org/PhysBio/8/026008/mmedia). Panel (*a*) shows the state of the colony at $t = 19.5$ (just before the friction is switched on at $t = 20$) when the colony shows a long-range nematic order. Panel (*b*) illustrates the disordered state after the bottom friction has been turned on ($t = 20.5$), and finally, panel (*c*) shows the partial re-establishment of order later at $t = 30$. Interestingly, in the nematically disordered regime, within the clusters cells are highly correlated in their position, so there is a certain evidence of a smectic order which is absent in the orientationally ordered quasi-nematic regime of figure 4(*a*). We can characterize the degree of orientational ordering along the x-axis by the scalar order parameter $\eta = [\langle \sin 2\phi \rangle^2 + \langle \cos 2\phi \rangle^2]^{1/2}$. The spacetime dependence of η in this run is shown in figure 4(*d*). As seen from this figure, as soon as the friction constant is turned on, the order parameter rapidly decreases in the middle of the trap, but then it gradually increases again. The origin of this re-ordering can be understood in the following way. Buckling instability evidently leads to more dense lateral packing of the cells (instead of 53 cellular columns across the domain before buckling, the system stabilizes at 70 columns after buckling). Thus, the lateral elastic modulus λ_{yy}, which is proportional to the number of cell per unit length along y, increases and that, as we have seen in the previous section, leads to the increase of the threshold for buckling instability. Even stronger buckling behavior is observed for smaller aspect ratios of the rods (see the supplementary information available at stacks.iop.org/PhysBio/8/026008/mmedia where similar results for $A = 4$ are presented).

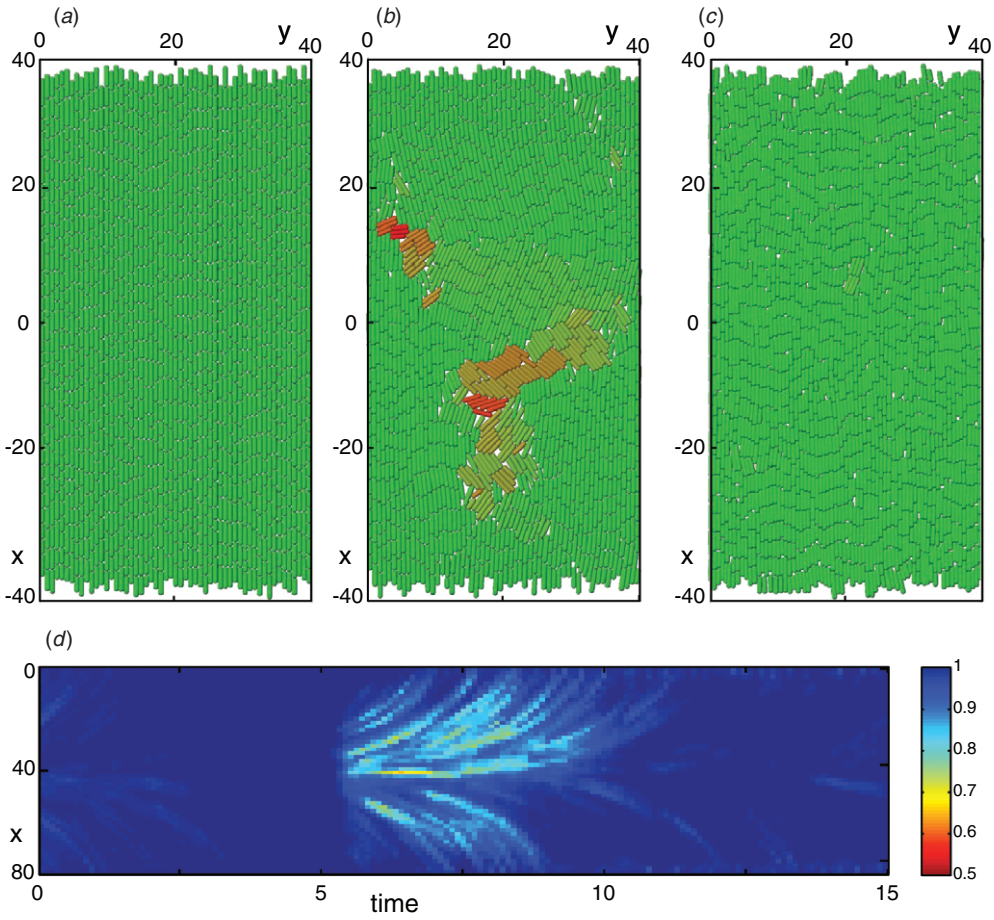

Figure 4. (*a*–*c*) Three still frames from a simulation of a growing colony in a 40 × 80 open trap at times (*a*) $t = 19.5$, (*b*) $t = 20.5$, (*c*) $t = 30$. The growth rate $a = 0.71$, maximum aspect ratio of cells $A = 6$ and the bottom friction $\mu = 10$ were turned on at $t = 20$. Coloring of the rods indicates rod's angle with respect to the *x*-axis: green $\phi = 0$, red $\phi = \pm\pi/2$. (d) Spacetime diagram of the magnitude of the order parameter averaged over the *y* dimension for the simulation exemplified in figure 4.

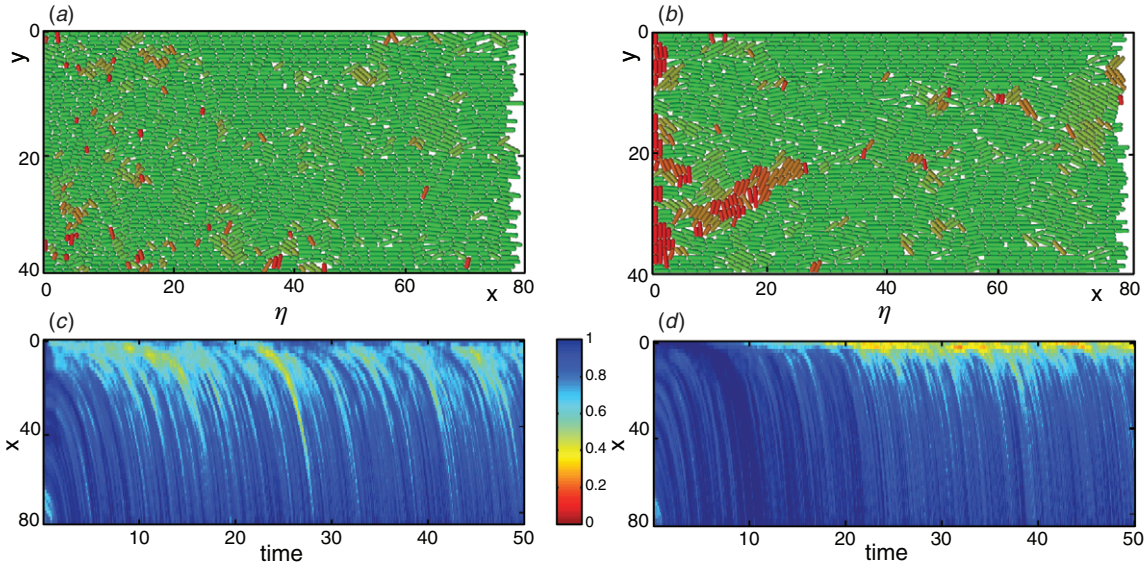

Figure 5. Still frames at time $t = 50$ (*a*, *b*) and spacetime diagrams (*c*, *d*) of the order parameter η (averaged over the transversal *y* coordinate) from simulations of a growing colony in a 40 × 80 side trap: (*a*, *c*) *x*-dependent mean cell size ($c = 0.5$); (*b*, *d*) *x*-independent mean cell size ($c = 0$).

In order to make a more direct connection with experiments, we also carried out simulations in a side-trap geometry, in which we also took into account the effect of nutrient depletion away from the open side of the trap. As observed experimentally, this depletion leads to slowing the cell growth and the reduction of the average cell size. We modeled this effect by the linear dependence of l_0 and the growth rate a on x: $\{l_0, a\} = \{l_0^0, a^0\}(1 - cx/L_x)$. We typically used $c = 0.5$ which indicates 50% reduction of cell growth near the back wall. We started simulations with a prepared nematic state in which all cells are densely packed and parallel to the x-axis. We also used a constant time-independent bottom friction coefficient $\mu = 13.5$. We observe that soon after the start of the run, buckling in the back of the trap occurs and, unlike the open-trap case, it appears to be persistent (see figures 5(*a*) and (*c*), and movie 5 in the supplementary information available at stacks.iop.org/PhysBio/8/026008/mmedia). In agreement with the experiment, the buckling instability originates near the back wall; however, the patches of disordered rods are then carried to the open boundary by the flow. As the cells move toward the open boundary, the disorder gradually decays, and the order parameter increases, as seen in figure 5(*c*). The size reduction in the back of the trap strongly contributes to the tendency of cells to buckle. To see this, we ran simulations with the same parameters except for $c = 0$, which corresponds to the uniform mean cell size. The effect of the cell size gradient can be clearly seen from comparing figures 5(*a*) and (*b*) and 5(*c*) and (*d*) (see also movie 6 in the supplementary information available at stacks.iop.org/PhysBio/8/026008/mmedia). In the latter case, a near-perfect nematic order is maintained for a long time and is only eventually broken by a rare fluctuation. The buckling is noticeably weaker; however, once it sets in, it also appears to be persistent. Unlike the variable size case, it mostly originates right at the back of the trap, where some rods eventually become parallel to the back wall and are forced to buckle because of the finite width of the trap. Since the x-component of the mean velocity near the back wall is zero, these rods linger near the back wall and serve as persistent sources of disorder which then propagates downstream toward the open boundary.

5. Concluding remarks

Bacteria in natural habitats typically move by rotating their flagellae and have developed complex biochemical mechanisms regulating their motion and collective behavior. However, in close proximity, such as in biofilms, bacteria usually lose their flagellae and become non-motile. Nevertheless, there are certain other physical mechanisms by which they interact and form multi-cellular structures. As we have shown earlier, the rod-like shape of many bacteria may lead to the establishment of local orientational order in bacterial colonies which is mediated by their growth and division. In this paper we described the buckling instability which limits the orientational order in sufficiently large bacterial colonies. We observed this effect in experiments with growing non-motile bacteria *E. coli* in large microfluidic traps and confirmed it in corresponding DES simulations. We also developed a continuum theory of the buckling instability based on the nematodynamic equations. The mechanism of the instability is related to the anisotropy of the stress tensor which builds up within the ordered growing colony. For a sufficiently strong anisotropy, the variations of the orientational order parameter (or simply orientation angle) begin to grow. In the limit of very small bending elasticity of the columns of rods, the growth rate of the instability increases with the wavenumber, and the instability leads to buckling at the smallest length scale which corresponds to the cell size. This buckling instability is a two-dimensional analog of the classical Euler instability of one-dimensional flexible rods under compression. We expect that the buckling instability may strongly affect the structure of bacterial populations in confined environments (such as surface-bound biofilms), if significant internal stresses develop there due to the cell growth. It may also affect the tissue growth and structure in multicellular organisms [3, 15].

Acknowledgments

This work was supported by the NIH (GM069811 and P50-GM085764) and UC-MEXUS. We are grateful to Dmitri Volfson for developing the original DES code and many useful discussions. DB and SOF thank UC San Diego for hospitality during part of this work. LT thanks UNAM for hospitality during his visits when some of this work was performed.

References

[1] Donlan R M 2002 *Emerg. Infect. Dis.* **8** 881–90
[2] Tolker-Nielsen T, Brinch U C, Ragas P C, Andersen J B, Jacobsen C S and Molin S 2000 *J. Bacteriol.* **182** 6482–9
[3] Drasdo D 2000 *Phys. Rev. Lett.* **84** 4244–7
[4] Goriely A and Ben Amar M 2005 *Phys. Rev. Lett.* **94** 198103
[5] Hall-Stoodley L and Stoodley P 2002 *Curr. Opin. Biotechnol.* **13** 228–33
[6] Volfson D, Cookson S, Hasty J and Tsimring L S 2008 *Proc. Natl Acad. Sci. USA* **105** 15346–51
[7] Mather W, Mondragón-Palomino O, Danino T, Hasty J and Tsimring L S 2010 *Phys. Rev. Lett.* **104** 208101
[8] Cho H J, Jönsson H, Campbell K, Melke P, Williams J W, Jedynak B, Stevens A M, Groisman A and Levchenko A 2008 *PLoS Biol.* **5** 2614–23
[9] Simha R A and Ramaswamy S 2002 *Phys. Rev. Lett.* **89** 58101
[10] Peruani F and Morelli L 2007 *Phys. Rev. Lett.* **99** 10602
[11] Landau L D and Lifshitz E M 1986 *Theory of Elasticity* 3rd edn (Oxford: Pergamon)
[12] Chaikin P M and Lubensky T C 2000 *Principles of Condensed Matter Physics* (Cambridge: Cambridge University Press)
[13] Abramoff M D, Magelhaes P J and Ram S J 2004 *Biophotonics Int.* **11** 36–42
[14] Landau L D and Lifshitz E M 1976 *Mechanics* 3rd edn (Oxford: Pergamon)
[15] Shraiman B I 2005 *Proc. Natl Acad. Sci. USA* **102** 3318–23